Journal of
Mechanics of
Materials and Structures

ANALYTICAL SOLUTIONS FOR DISPLACEMENTS AND STRESSES IN FUNCTIONALLY GRADED THICK-WALLED SPHERES SUBJECTED TO A UNIDIRECTIONAL OUTER TENSION

Chenyi Zheng and Changwen Mi

Volume 15, No. 5 December 2020

msp

JOURNAL OF MECHANICS OF MATERIALS AND STRUCTURES
Vol. 15, No. 5, 2020
https://doi.org/10.2140/jomms.2020.15.585

ANALYTICAL SOLUTIONS FOR DISPLACEMENTS AND STRESSES IN FUNCTIONALLY GRADED THICK-WALLED SPHERES SUBJECTED TO A UNIDIRECTIONAL OUTER TENSION

CHENYI ZHENG AND CHANGWEN MI

In the context of infinitesimal theory of elasticity, we derived analytical solutions for displacements and stresses in functionally graded thick-walled spheres under the application of a uniaxial outer tension. While the shear modulus in the graded sphere is allowed to vary as a power-law function of radial coordinate, the Poisson's ratio is treated as a constant. The semiinverse method of elasticity is first employed for proposing correct function forms of the radial and longitudinal displacements. The elastostatic Navier's equations of the power-law graded sphere lead to a system of second-order differential equations of the Euler type. The order is then reduced and the system is recast into a first-order differential matrix equation. Analytical solutions are subsequently developed by the coupling of differential equation and eigenvalue theories. Successfully solving this particular problem provides a valid analytical solution scheme for exploring elastic fields in graded hollow spheres subjected to nonhydrostatic boundary loads. In order to examine the effects of the power-law gradation and the radii ratio of the thick-walled sphere on stress distributions and stress concentration factors, extensive parametric studies are conducted. Analytical solutions of the graded thick-walled sphere are further compared with those of the homogeneous case as well as with the numerical results due to finite element modelings. The obtained results show that the property gradation significantly affects stress distributions through the thickness direction of the graded thick-walled sphere. When the shear modulus is designed as an increasing function of the radial coordinate, the high stress zone conventionally occurring near the inner boundary of homogeneous thick-walled spheres tends to shift toward to the outer surface vicinity. For a given radii ratio, an optimal power-law gradation leading to the lowest stress concentration factor can always be identified. The proposed method of solution and the obtained results are useful for the design and manufacturing of better performing spherical vessels.

1. Introduction

It is a well accepted fact that stress concentration (SC) is an inherent threatening to the structural integrity of pressure vessels. The concentration of stresses typically occurs near the reentrant boundaries, geometric defects and points of force application. The maximum stress may be as high as several times of the applied load. In the literature, this ratio is defined as the stress concentration factor (SCF) for a certain combination of structure and loading conditions [Barber 1992]. Scientists and engineers have been working hard to reduce and avoid SC both in theory and in engineering practice. One idea is to replace

Changwen Mi is the corresponding author.

Keywords: functionally graded spheres, unidirectional loading, analytical solution, stress concentration factor, finite element modeling.

the completely homogeneous material of an engineering component with functionally graded materials (FGMs). Within the context of mechanics, FGMs are a relatively new design strategy to regulate and optimize the stress distributions in engineering materials and structures. The most typical example is the combination of ceramic and metallic materials [Evci and Gülgeç 2018]. Fukui and Yamanaka [1992] evaluated the stresses in graded thick-walled tubes made by the combination of a matrix composed of three low-modulus materials and high-modulus particles. The gradation profile through the tube thickness is controlled by the volume fraction of the reinforcement particles. Suresh et al. [1999] demonstrated that a thin coating made of graded alumina-glass composite significantly reduces the sliding contact damage of a polycrystalline alumina surface. As a direct result of the replacement, the modulus of elasticity is allowed to vary through one or more spatial dimensions. In any theory of mechanics, both deformations and stresses are closely related to elastic modulus. It is hoped that, through the proper regulation of elastic modulus, stresses may redistribute following a desired pattern.

Materials and structures with graded modulus of elasticity [Birman and Byrd 2007; Ghayesh and Farajpour 2019] have been designed and manufactured since 1980s and gained many applications in contact mechanics [Suresh et al. 1999; Yan et al. 2019; Yan and Mi 2019] and fracture mechanics [Jin and Batra 1996]. Tutuncu and Ozturk [2001] derived closed-form displacements and stresses of graded cylindrical and spherical vessels under internal pressure alone. The shear modulus was also assumed to vary as a power-law function through the wall thickness. Tutuncu [2007] further derived power series solutions to a thick-walled cylinder under the application of internal pressure only. This time, the elastic modulus of the cylinder is assumed to be an exponential function of the radial coordinate. Due to this change of gradation function, an analytical solution to the axisymmetric equilibrium equations of the radial displacement becomes more difficult. As a result, the author presented the solution in the form of power series by employing the Frobenius method. The closed-form solution of this problem was later derived by Nejad et al. [2016] in the plain strain condition. Atashipour et al. [2014] solved the elastic fields in a homogeneous hollow sphere internally coated with a graded layer under hydrostatic boundary pressures. Analytical solutions were derived for graded coating with both linearly and exponentially-varying shear modulus. More recently, Evci and Gülgeç [2018] developed an analytical solution in a graded hollow cylinder whose thermoelastic material properties are assumed to be power functions of the radial coordinate.

As a powerful numerical approach, finite element (FE) analysis has also been employed for solving cylindrical and spherical vessels under the application of hydrostatic loads. Nejad et al. [2016] compared their analytical solutions with those resulting from the FE modelings. Ghannad and Nejad [2012] first derived a complete analytical solution to thick-walled spheres with power-law gradation of elastic modulus. The distribution of displacements and stresses were compared with those obtained by the FE method. Apart from completely graded vessels [Ghannad 2013; Dryden and Batra 2013; Xin et al. 2014; Yang et al. 2015], thick-walled cylinders and spheres reinforced with a graded coating have also been studied. Sburlati and Cianci [2015] investigated the effects of a graded interphase zone bridging a spherical inclusion and a matrix subjected to a far-field pressure loading. The same structure under the application of a uniform heating has also been considered [Sburlati et al. 2017].

All works reviewed above dealt with hollow cylinders and spheres under the application of hydrostatic pressures. Nonhydrostatic traction loads did not receive reasonable attentions until the last decade. Based on the multiple isoparametric FE formulation, Kubair and Bhanu-Chandar [2008] numerically

determined the SCF in a cylindrical panel containing a circular hole under the application of a far-field uniaxial tension. Since the problem was numerically solved, both the power-law and exponential variations of elastic modulus were considered. By the use of Airy stress function approach, Nie and Batra [2010] derived analytical solutions of a graded hollow cylinder under normal and shear tractions applied at its both boundaries. Mohammadi et al. [2011] evaluated the SCFs around a circular hole in a radially graded plate subjected to either equal-biaxial or pure shear far-field tractions. Kubair [2013] further derived closed-form elastic fields for the same panel geometry under the application of a far-field antiplane shear loading. This time, only the exponential variation of elastic modulus was considered. Sburlati [2013] derived an analytical solution to a circularly voided homogeneous plate reinforced by a graded ring under the application of a far-field uniaxial tension. On this basis, Sburlati et al. [2014] further considered the same geometry under the application of four different far-field loads, including uniaxial tension, equal-biaxial tension and two forms of pure shear. Yang and Gao [2016] evaluated the SCFs in a homogenous panel containing an elliptic hole that is reinforced by a graded coating layer. Arbitrary loads and property gradations in the graded coating can be considered. Le [2017] developed an asymptotically exact two-dimensional theory for functionally graded piezoelectric shells by synthesizing the variational and asymptotic methods. As an application, the analytical solution to the forced vibration of a graded piezoceramic cylindrical shell excited by a harmonic voltage was derived. Li et al. [2018] considered a homogeneous thick-walled cylinder reinforced by a graded coating subjected to an arbitrary biaxial outer loading. The effects of the graded coating on the reduction of SC and the optimization of stress distributions were analyzed.

The references reviewed above demonstrate that fewer works have devoted to graded thick-walled spheres subjected to nonhydrostatic loads. Poultangari et al. [2008] first proposed a series solution for a power-law graded hollow sphere under the application of nonhydrostatic thermomechanical loads. Later, the same research group further employed this solution method for solving the piezothermoelastic fields in standalone graded hollow spheres [Jabbari et al. 2013] and graded hollow spheres perfectly bonded by piezoelectric layers [Barati and Jabbari 2015; Jabbari et al. 2017]. Also based on the series solution principle, Bayat and EkhteraeiToussi [2015] investigated the thermomechanical fields in a transversely isotropic hollow sphere rotating at a constant angular velocity. Sburlati et al. [2018] derived elastic solutions in an inhomogeneous spherical interphase separating a solid spherical inclusion and a finite matrix. By assuming a power-law variation in shear modulus and a constant Poisson's ratio, closed-form solutions to both hydrostatic and pure-shear outer tractions were developed. In another recent paper, Zheng et al. [2019] developed a semianalytical solution to a homogeneous hollow sphere interiorly coated with a graded layer. Although a uniaxial outer tension was considered, displacements and stresses of the graded coating were not directly solved within the elasticity theory of an inhomogeneous medium. Instead, the solution was approximated by its homogeneous counterpart through discretizing the graded coating into a few perfectly bonded homogeneous sublayers [Yang et al. 2009; Yang and Gao 2016].

The goal of this work is to continue the efforts in this line of research. Here, we consider the fundamental problem of a graded thick-walled sphere under the application of a uniaxial outer tension. The hollow sphere is assumed to possess power-law variation of shear modulus through its thickness. Since the Poisson's ratio is treated as a constant, Young's modulus of the isotropic thick-walled sphere also varies by the same power-law function. Following the basic equations of an inhomogeneous elastic medium, the boundary value problem is solved by the collective use of semiinverse method of elasticity

theory, reduced-order method of differential equations and eigenvalue theory. In addition to analytical solutions, FE modelings are also implemented to validate the correctness of stress distributions and SCFs. The remainder of this paper is structured as follows. Section 2 describes the mechanical formulation and analytical solutions to the graded thick-walled sphere under the application of a uniaxial outer tension. In Section 3, extensive parametric studies are conducted for illustrating the effects of property gradation and radii ratio on stress distributions and reduction of SCFs. FE modeling results are also presented to validate the correctness of analytical solutions. Finally, in Section 4, concluding remarks are delivered.

2. Method of solution

Figure 1 shows a graded thick-walled sphere under the application of a unidirectional outer tension of magnitude T. The inner and outer radius of the sphere are represented by a and b, respectively. Given the spherical symmetry of the geometry, spherical coordinates (R, φ, θ) are employed for the subsequent mechanical formulation, where R, φ and θ denote the radial, longitudinal and latitudinal coordinates, respectively. In view of its limited influence on stress distributions, the Poisson's ratio (ν) of the graded sphere is assumed to be a constant [Sburlati 2013]. The shear modulus of the graded sphere varies as a power-law function of the radial coordinate:

$$G = G_o R^m / b^m, \tag{1}$$

where G_o denotes the shear modulus value at the outer boundary of the graded sphere and m is the grading index, indicating the varying gradient of the shear modulus. It is worth noting that shear modulus instead of Young's modulus has been used in Equation (1). For the method of displacement potentials used in this work, the combination of shear modulus and Poisson's ratio is able to formulate the solution in the simplest form than any other combinations of elastic constants.

In spherical coordinates, the unidirectional tension applied at the outer boundary of the graded sphere can be expressed as

$$\frac{\sigma_R(b,\zeta)}{T} = \zeta^2, \quad \frac{\sigma_{R\varphi}(b,\zeta)}{T} = -\zeta\sqrt{1-\zeta}, \tag{2}$$

where $\zeta = \cos\varphi$. At the inner surface of the graded sphere, both the normal and the shear tractions are zero:

$$\sigma_R(a,\zeta) = 0, \quad \sigma_{R\varphi}(a,\zeta) = 0. \tag{3}$$

In spite of the dependence of shear modulus on the radial coordinate, the governing equations for the graded thick-walled sphere are not different from those for a homogeneous medium. The strain-displacement relations are given by

$$\begin{gathered}\varepsilon_R = \frac{\partial u_R}{\partial R}, \quad \varepsilon_\varphi = \frac{u_R}{R} - \frac{\sqrt{1-\zeta^2}}{R}\frac{\partial u_\varphi}{\partial \zeta}, \quad \varepsilon_\theta = \frac{u_R}{R} + \frac{\zeta u_\varphi}{R\sqrt{1-\zeta^2}}, \\ \varepsilon_{R\varphi} = \frac{1}{2}\left(\frac{\partial u_\varphi}{\partial R} - \frac{\sqrt{1-\zeta^2}}{R}\frac{\partial u_R}{\partial \zeta} - \frac{u_\varphi}{R}\right).\end{gathered} \tag{4}$$

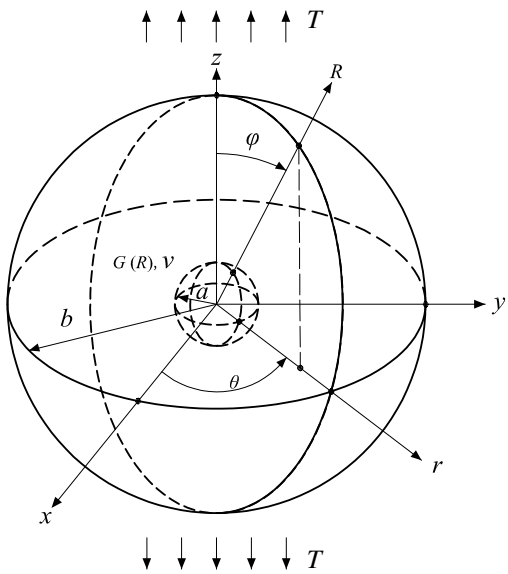

Figure 1. A thick-walled sphere with radially graded shear modulus under the application of a unidirectional outer tension.

In terms of the inhomogeneous shear modulus (1), the linear constitutive relations still assume the form

$$\sigma_R=\frac{2G(R)\nu}{1-2\nu}(\varepsilon_R+\varepsilon_\theta+\varepsilon_\varphi)+2G(R)\varepsilon_R,\quad \sigma_\varphi=\frac{2G(R)\nu}{1-2\nu}(\varepsilon_R+\varepsilon_\theta+\varepsilon_\varphi)+2G(R)\varepsilon_\varphi,$$
$$\sigma_\theta=\frac{2G(R)\nu}{1-2\nu}(\varepsilon_R+\varepsilon_\theta+\varepsilon_\varphi)+2G(R)\varepsilon_\theta,\quad \sigma_{R\varphi}=2G(R)\varepsilon_{R\varphi}. \tag{5}$$

In the absence of body forces, the axisymmetric equations of equilibrium in spherical coordinates are given by [Barber 1992]

$$\frac{\partial\sigma_R}{\partial R}+\frac{\zeta\sigma_{R\varphi}}{R\sqrt{1-\zeta^2}}-\frac{\sqrt{1-\zeta^2}}{R}\frac{\partial\sigma_{R\varphi}}{\partial\zeta}+\frac{2\sigma_R-\sigma_\theta-\sigma_\varphi}{R}=0,$$
$$\frac{\zeta(\sigma_\varphi-\sigma_\theta)}{R\sqrt{1-\zeta^2}}-\frac{\sqrt{1-\zeta^2}}{R}\frac{\partial\sigma_\varphi}{\partial\zeta}+\frac{\partial\sigma_{R\varphi}}{\partial R}+\frac{3\sigma_{R\varphi}}{R}=0. \tag{6}$$

In view of the traction distributions (2), the constitutive equations (5) and the strain-displacement relations (4), it can be inferred that the radial and longitudinal displacements in the graded sphere must follow the form

$$u_R=P_1(R)+\zeta^2P_2(R),\quad u_\varphi=\zeta\sqrt{1-\zeta^2}P_3(R). \tag{7}$$

Only when the displacements are in these forms, the traction boundary conditions (2) can possibly be satisfied. By the substitution of the proposed displacements (7) back into the three sets of governing equations (4), (5) and (6), the equations of equilibrium of the graded sphere become

$$\frac{G_o R^{m-2}}{(1-2\nu)\, b^m}\left(H_1(R)+\zeta^2 H_2(R)\right)=0, \quad \frac{G_o R^{m-2}}{(1-2\nu)\, b^m}\zeta\sqrt{1-\zeta^2}H_3(R)=0, \tag{8}$$

where $H_1(R)$, $H_2(R)$ and $H_3(R)$ are functions of the radial coordinate:

$$\begin{aligned} H_1(R) = &-2(1-\nu)\, P_1''(R)R^2 - \left[2(1-\nu)(m+2)\, P_1'(R) - P_3'(R)\right] R \\ &+4(1-\nu-m\nu)\, P_1(R) - 2(1-2\nu)\, P_2(R) - (3-2\nu(m+2))\, P_3(R), \end{aligned} \tag{9a}$$

$$\begin{aligned} H_2(R) = &-2(1-\nu)\, P_2''(R)R^2 - \left[2(1-\nu)(m+2)\, P_2'(R) + 3P_3'(R)\right] R \\ &+2(5-2\nu(m+4))\, P_2(R) + 3(3-2\nu(m+2))\, P_3(R), \end{aligned} \tag{9b}$$

$$\begin{aligned} H_3(R) = &-(1-2\nu)\, P_3''(R)R^2 - \left[(1-2\nu)(m+2)\, P_3'(R) - 2P_2'(R)\right] R \\ &+2(4(1-\nu) - m(1-2\nu))\, P_2(R) + (12(1-\nu) + m(1-2\nu))\, P_3(R). \end{aligned} \tag{9c}$$

Since $\zeta = \cos\varphi$ may take any value within the closed interval $[-1, 1]$, equations (8) can be satisfied if and only if

$$H_1(R)=0, \quad H_2(R)=0, \quad H_3(R)=0. \tag{10}$$

These are three coupled differential equations of Euler type with respect to the three unknown functions $P_1(R)$, $P_2(R)$ and $P_3(R)$. By replacing the radial coordinate with $R=e^t$ in (9), equations (10) reduce to a system of coupled ordinary differential equations:

$$\begin{aligned} &-2(1-\nu)\, P_1''(t) - 2(1-\nu)(m+1)\, P_1'(t) + P_3'(t) \\ &\quad +4(1-\nu-m\nu)\, P_1(t) - 2(1-2\nu)\, P_2(t) - (3-2\nu(m+2))\, P_3(t) = 0, \end{aligned} \tag{11a}$$

$$\begin{aligned} &-2(1-\nu)\, P_2''(t) - 2(1-\nu)(m+1)\, P_2'(t) - 3P_3'(t) \\ &\quad +2(5-2\nu(m+4))\, P_2(t) + 3(3-2\nu(m+2))\, P_3(t) = 0, \end{aligned} \tag{11b}$$

$$\begin{aligned} &-(1-2\nu)\, P_3''(t) + 2P_2'(t) - (1-2\nu)(m+1)\, P_3'(t) \\ &\quad +(8(1-\nu) + 2m(1-2\nu))\, P_2(t) + (12(1-\nu) + m(1-2\nu))\, P_3(t) = 0. \end{aligned} \tag{11c}$$

These three ordinary differential equations may further be expressed in matrix form as

$$\mathrm{d}\boldsymbol{W}/\mathrm{d}t = \boldsymbol{Q}\boldsymbol{W}, \tag{12}$$

with $\boldsymbol{W}$ denoting a column vector composed of the three unknown functions and their derivatives:

$$\boldsymbol{W} = \left[\, P_1(t) \;\; P_2(t) \;\; P_3(t) \;\; P_1'(t) \;\; P_2'(t) \;\; P_3'(t) \,\right]^T, \tag{13}$$

and $\boldsymbol{Q}$ representing a 6×6 square matrix:

$$\boldsymbol{Q} = \begin{bmatrix} 0 & 0 & 0 & 1 & 0 & 0 \\ 0 & 0 & 0 & 0 & 1 & 0 \\ 0 & 0 & 0 & 0 & 0 & 1 \\ \frac{2(1-\nu-m\nu)}{1-\nu} & -\frac{1-2\nu}{1-\nu} & -\frac{3-2\nu(2+m)}{2(1-\nu)} & -1-m & 0 & \frac{1}{2(1-\nu)} \\ 0 & \frac{5-2\nu(4+m)}{1-\nu} & \frac{9-6\nu(2+m)}{2(1-\nu)} & 0 & -1-m & -\frac{3}{2(1-\nu)} \\ 0 & \frac{8(1-\nu)+2m(1-2\nu)}{1-2\nu} & \frac{12(1-\nu)+m(1-2\nu)}{1-2\nu} & 0 & \frac{2}{1-2\nu} & -1-m \end{bmatrix}. \tag{14}$$

Equation (12) can be solved by coupling the solutions of an inhomogeneous first-oder differential equation and eigenvalue problems of a square matrix. To this end, the six eigenvalues of the coefficient matrix $\boldsymbol{Q}$ must first be found:

$$\lambda_{1,2} = \frac{k_1 \pm \sqrt{k_2}}{k_0}, \quad \lambda_{3,4} = \frac{k_1 \pm \sqrt{k_3 - 2\sqrt{k_4}}}{k_0}, \quad \lambda_{5,6} = \frac{k_1 \pm \sqrt{k_3 + 2\sqrt{k_4}}}{k_0}, \tag{15}$$

where k_0 through k_4 are five dimensionless parameters that can be expressed in terms of Poisson's ratio and the grading index:

$$\begin{aligned}
k_0 &= 2(1-\nu)(1-2\nu),\\
k_1 &= -(1-\nu)(1-2\nu)(m+1),\\
k_2 &= (1-\nu)(1-2\nu)^2\big((1-\nu)(9+m^2)+2m(1-5\nu)\big),\\
k_3 &= m^2(1-\nu)^2(1-2\nu)^2 + 4m(1-\nu)(1-2\nu)^3 + 29 - 174\nu + 377\nu^2 - 348\nu^3 + 116\nu^4,\\
k_4 &= (1-\nu)^2(1-2\nu)^4\big(m^2(1-22\nu+25\nu^2) + 4m(11-36\nu+25\nu^2) + 100(1-\nu)^2\big).
\end{aligned} \tag{16}$$

For Poisson's ratio $\nu \in (0, 0.5)$, all six eigenvalues of the coefficient matrix (15) are real for the grading index $0 < m \leq 2$. As a result, the general solution of the differential matrix equation (12) can be given by the linear combination of the six eigenvalues:

$$P_1(t) = \sum_{k=1}^{6} \frac{A_k}{a^{\lambda_k - 1}} e^{\lambda_k t}, \quad P_2(t) = \sum_{k=1}^{6} \frac{B_k}{a^{\lambda_k - 1}} e^{\lambda_k t}, \quad P_3(t) = \sum_{k=1}^{6} \frac{C_k}{a^{\lambda_k - 1}} e^{\lambda_k t}. \tag{17}$$

In these equations, replacing the independent variable t with $\ln R$ leads to

$$P_1(R) = \sum_{k=1}^{6} \frac{A_k}{a^{\lambda_k - 1}} R^{\lambda_k}, \quad P_2(R) = \sum_{k=1}^{6} \frac{B_k}{a^{\lambda_k - 1}} R^{\lambda_k}, \quad P_3(R) = \sum_{k=1}^{6} \frac{C_k}{a^{\lambda_k - 1}} R^{\lambda_k}. \tag{18}$$

Recall that, altogether, these three functions must satisfy the two equations of equilibrium (8). The three groups of coefficients, A_k, B_k and C_k, are therefore not independent. By the substitution of (18) back into (8), we can obtain

$$B_k = S(\lambda_k) A_k, \quad C_k = L(\lambda_k) A_k, \tag{19}$$

where $S(\lambda_k)$ and $L(\lambda_k)$ are given by

$$\begin{aligned}
S(\lambda_k) &= \frac{\big(2m\nu - (1-\nu)(2-(m+1)\lambda_k - \lambda_k^2)\big)\big(12(1-\nu) + (1-2\nu)(m - (m+1)\lambda_k - \lambda_k^2)\big)}{2\big((1-\nu)(m+4\nu-6\nu m - 2\nu(m+1+\lambda_k)\lambda_k) - m^2\nu(1-2\nu)\big)},\\
L(\lambda_k) &= -\frac{\big(2m\nu - (1-\nu)(2-(m+1)\lambda_k - \lambda_k^2)\big)\big(4(1-\nu) + m(1-2\nu) + \lambda_k\big)}{(1-\nu)\big(m+4\nu-6\nu m - 2\nu(m+1+\lambda_k)\lambda_k\big) - m^2\nu(1-2\nu)}.
\end{aligned} \tag{20}$$

With equations (19), the 18 unknown coefficients have reduced to only six: A_1, A_2, A_3, A_4, A_5, A_6. They remain to be determined by implementing the traction boundary conditions at the outer surface (2) and the inner surface (3) of the graded sphere.

Given the general solutions of the three unknown functions (18) in the radial and longitudinal displacement (7), it is straightforward to derive the general expressions of displacements. The four nontrivial

strain components can be further derived from the strain-displacement relations (4). Finally, with the help of the shear modulus distribution (1), the radial and longitudinal stresses (5) can be recast

$$\frac{\sigma_R}{T} = \frac{R^m}{b^m}\sum_{k=1}^{6} A_k\left(\alpha_k + \zeta^2\beta_k\right)\frac{a^{1-\lambda_k}}{R^{1-\lambda_k}}, \quad \frac{\sigma_{R\varphi}}{T} = \zeta\sqrt{1-\zeta^2}\frac{R^m}{b^m}\sum_{k=1}^{6} A_k\gamma_k\frac{a^{1-\lambda_k}}{R^{1-\lambda_k}}, \tag{21}$$

where α_k, β_k and γ_k $(k = 1, \ldots, 6)$ are all dimensionless functions of the shear modulus G_o, the magnitude of the applied uniaxial tension T, Poisson's ratio ν, the grading index m and the eigenvalues λ_k:

$$\alpha_k = \frac{2G_o}{(1-2\nu)\,T}\left((1-\nu)\,\lambda_k + \nu\,(2 - L\,(\lambda_k))\right), \tag{22a}$$

$$\beta_k = \frac{2G_o}{(1-2\nu)\,T}\left((1-\nu)\,\lambda_k S\,(\lambda_k) + \nu\,(2S\,(\lambda_k) + 3L\,(\lambda_k))\right), \tag{22b}$$

$$\gamma_k = -\frac{G_o}{T}\left(2S\,(\lambda_k) + (1-\lambda_k)\,L\,(\lambda_k)\right). \tag{22c}$$

Equations (21) are valid expressions of the radial and shear stresses for any graded hollow sphere with the shear modulus distribution given by (1). The six unknown coefficients $(A_1, \ldots, A_6)$ are adjustable parameters that remain to be determined by satisfying specific traction or displacement boundary conditions at both the inner and the outer surfaces of the hollow sphere. Upon implementing the uniaxial outer tension condition (2) at $R = b$ and the traction-free condition (3) at $R = a$, we arrive at four simultaneous algebraic equations. In these equations, equating those terms independent of the variable ζ, preceding ζ^2 and $\zeta\sqrt{1-\zeta^2}$ leads to six linear equations about the six unknown coefficients $(A_1, \ldots, A_6)$. This set of equations may be restructured into a single matrix equation:

$$[\boldsymbol{U}]\,\{\boldsymbol{X}\} = \{\boldsymbol{V}\}, \tag{23}$$

where the components of the 6×6 square matrix $\boldsymbol{U}$ are given by

$$U_{1k} = \alpha_k, \quad U_{2k} = \beta_k, \quad U_{3k} = \gamma_k, \quad U_{4k} = \frac{\alpha_k a^{1-\lambda_k}}{b^{1-\lambda_k}}, \quad U_{5k} = \frac{\beta_k a^{1-\lambda_k}}{b^{1-\lambda_k}}, \quad U_{6k} = \frac{\gamma_k a^{1-\lambda_k}}{b^{1-\lambda_k}}; \tag{24}$$

$\boldsymbol{X}$ is column vector composed of the six unknowns

$$\boldsymbol{X} = \left\{\begin{array}{cccccc} A_1 & A_2 & A_3 & A_4 & A_5 & A_6 \end{array}\right\}^T; \tag{25}$$

and $\boldsymbol{V}$ is also a column vector with the simple form

$$\boldsymbol{V} = \left\{\begin{array}{cccccc} 0 & 0 & 0 & 0 & 1 & -1 \end{array}\right\}^T. \tag{26}$$

The algebraic matrix equation (23) is linear with respect to the six unknowns. As a result, its solution procedure follows the standard linear algebra algorithm. The six unknowns can be easily found:

$$A_k = (\boldsymbol{U}^{-1})_{k5} - (\boldsymbol{U}^{-1})_{k6} = \frac{(\boldsymbol{U})'_{5k} - (\boldsymbol{U})'_{6k}}{|\boldsymbol{U}|}, \tag{27}$$

where $\boldsymbol{U}^{-1}$, $\boldsymbol{U}'$ and $|\boldsymbol{U}|$ are the inverse, matrix of cofactors and determinant of the coefficient matrix $\boldsymbol{U}$. Since there are only two nonzero components in the column vector $\boldsymbol{V}$, only the last two rows of the matrices of inverse and cofactors are required in the solutions.

In view of equations (24), closed-form expressions of the unknowns A_k can be further developed without difficulty. Nonetheless, the results are quite lengthy. For brevity, they are not presented in the manuscript. Interested readers are invited to implement the solution procedure in a symbolic mathematical software.

3. Results and discussion

In the last section, we developed an analytical solution to a graded thick-walled sphere subjected to a uniaxial outer tension. For brevity, the closed-form expressions of the final results were not presented. The purpose of the present section is to further explore the effects of the power-law grading index m and the radii ratio b/a on both the stress distributions and the SCFs in terms of numerical experiments.

As can be concluded from previous studies on graded cylinders and spheres [Sburlati 2013], the effects of Poisson's ratio on stress fields are inessential when compared with those of the shear modulus. Xin et al. [2014] further provided one theoretical foundation for justifying the assumption of constant Poisson's ratio extensively adopted in the literature. They indicated that, although the effects of Poisson's ratio on the radial displacement of a thick-walled tube under internal pressure are appreciable, those on stresses are not obvious. As a result, the Poisson's ratio was fixed as $\nu = 0.3$ in all our case studies.

As a means of verifying and validating the correctness of the developed theoretical formulation, FE solutions calculated through ABAQUS/Standard software were also prepared for most examples. In all numerical experiments, the shear modulus at the outer boundary of the thick-walled sphere was taken as $G_o = 80\,\text{GPa}$. The magnitude of the uniaxial outer tension was chosen as $T = 50\,\text{MPa}$.

Previous studies demonstrate that high moduli of elasticity near the inner boundary of a thick-walled sphere tend to worsen stress concentrations [Zheng et al. 2019]. In order to relieve the stress concentrations that typically occur at the inner surface of hollow spheres, their modulus of elasticity should be designed as an increasing function of the radial coordinate. In other words, near the conventional stress concentration zone, soft materials should be employed. For regions far way from the void, hard materials can still be used. This design principle helps to drive the high-stress zone near the spherical void toward to the outer boundary of the thick-walled sphere. On the basis of such an argument, only positive grading indices should be considered in (1). For the special case of zero grading, the proposed graded thick-walled sphere of course reduces to a completely homogeneous medium.

Figure 2 shows the distribution of the longitudinal stress along the inner surface of the graded thick-walled sphere for the particular radii ratio $b/a = 3$. To investigate the effects of modulus inhomogeneity, five positive grading indices were considered. For completeness, the classical solution of a homogeneous thick-walled sphere is included in the figure. It can be seen from the figure that, the introduction of an inhomogeneous shear modulus does not change the distribution pattern of the longitudinal stress along the inner boundary. For any grading index, the maximum value of this stress component still occurs along the equator of the inner surface ($\varphi = \pi/2, 0 \le \theta \le 2\pi$). Due to symmetry, the minimum value of the longitudinal stress takes place at both poles of the inner surface ($\varphi = 0, \pi$). The longitudinal stress varies monotonically with the grading index. As m increases, the magnitude of both the maximum and the minimum longitudinal stress decreases, indicating the desired effects of modulus inhomogeneity on stress concentrations.

Because, on the inner surface of a graded thick-walled sphere, stress concentrations always occur

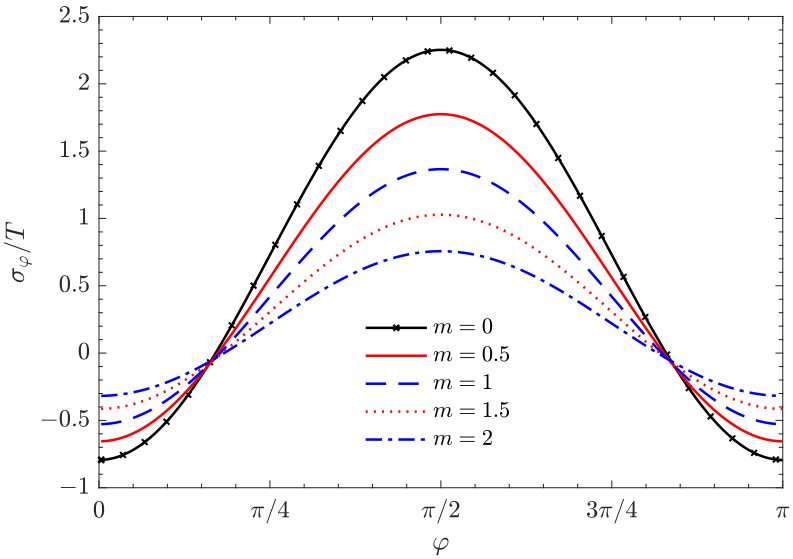

Figure 2. Variation of dimensionless longitudinal stress along the inner surface of the graded thick-walled sphere for five grading indices ($b/a = 3$, $R = a$).

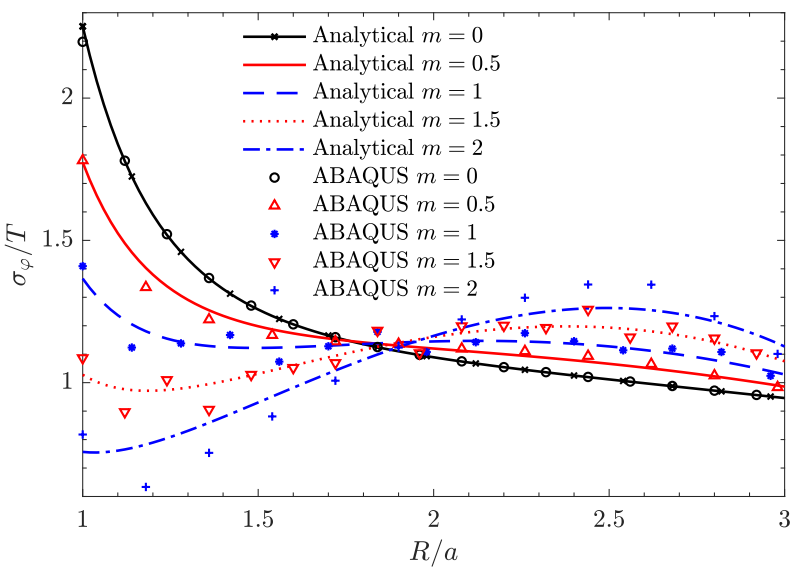

Figure 3. Variation of dimensionless longitudinal stress with radial distance for five grading indices ($b/a = 3$, $\varphi = \pi/2$).

along the equator, it is informative to further examine the variation of the longitudinal stress between the inner and the outer equators of the sphere (Figure 3). The same five grading indices as studied in Figure 2 were considered. It is now even more obvious that, at the inner surface of the graded sphere, the longitudinal stress decays monotonically with increased grading index. For the particular thickness ratio ($b/a = 3$), the highest stress concentration still occurs at the equator of the inner surface when $m = 0.5$

and 1. In particular, when $m = 0.5$, the longitudinal stress decays rapidly with the radial distance from the center of the sphere. However, the rate of decay becomes much slower as the grading index increases to $m = 1$. Near the middle interface of the sphere, a stress plateau can be clearly observed. In addition to the highest longitudinal stress occurring at the inner surface of the sphere, another local stress maximum has also appeared at $R/a = 2.12$. The variation of the longitudinal stress is no longer monotonic. Two points of inflection can be observed. As the grading index further increases to $m = 1.5$, the maximum longitudinal stress in the thick-walled sphere has shifted from its inner surface to $R/a = 2.38$. As a result, the high stress zone in the thick-walled sphere has changed to the vicinity of the outer surface. For the highest considered grading index $m = 2$, this observation becomes even more clear. The inner surface of the thick-walled sphere has become a global minimum of the longitudinal stress. For the five grading indices, the longitudinal stress values at the outer surface of the graded thick-walled sphere are all close to the applied uniaxial tension.

For comparison purpose, in Figure 3, we have also presented FE solutions for all five grading indices. The FE solutions were calculated in ABAQUS/Standard software by employing the sublayer method, in which a unidirectionally graded medium is divided into multiple homogeneous layers [Zheng et al. 2019; Liu et al. 2018; Yan et al. 2019; Yan and Mi 2019]. For brevity, the implementation details are not repeated here. It can be seen from the figure that the analytical and FE solutions agree quite well for small grading indices, validating the correctness of both methods. It is also noted that the relative error between two solutions increases with the grading index. This behavior may be attributed to three factors. First, in the FE modelings, all graded spheres were approximated with ten homogeneous sublayers. As the grading index becomes higher, the shear modulus of the graded sphere varies faster, calling for a finer FE simulation scheme. Second, among all four non-trivial components, the longitudinal stress is the most important one. The largest magnitude of latitudinal, radial and shear stresses does not exceed the applied external load, as will be presented shortly in this section. Third, for a thick-walled hollow sphere, stress concentration is most severe along its inner surface.

In Table 1, we tabulate the SCF and its appearing location for a few grading indices in the range of $0 \le m \le 2$. The rate of reduction of the SCFs as compared with that of the classical solution is also given in the table. Consistent with the stress distributions shown in Figure 3, for $m \le 1.25$, the maximum longitudinal stress always occurs at the inner surface ($R/a = 1$) of the graded thick-walled sphere and continues to decrease with the grading index. As the grading index increases to $m = 1.5$, the maximum longitudinal stress does not occur at the inner surface anymore. The location at which the maximum longitudinal stress occurs has shifted to $R/a = 2.38$ and a reduction rate of 46.8% is achieved. This value is lower than the one corresponding to the grading index $m = 1.25$. It can therefore be anticipated that an optimal grading index (m_{opt}) must exist in the interval $1.25 < m < 1.5$. For such

m	0	0.25	0.5	0.75	1	1.25	1.5	1.75	2	$m_{\text{opt}} = 1.28$
SCF	2.252	2.005	1.774	1.561	1.366	1.188	1.197	1.229	1.262	1.173
Location (R/a)	1	1	1	1	1	1	2.38	2.44	2.50	1 & 2.30
Reduction rate	0	11.0%	21.2%	30.7%	39.3%	47.2%	46.8%	45.4%	44.0%	47.9%

Table 1. The stress concentration factor and its location for a few graded thick-walled spheres under the application of a uniaxial outer tension ($b/a = 3$, $\nu = 0.3$).

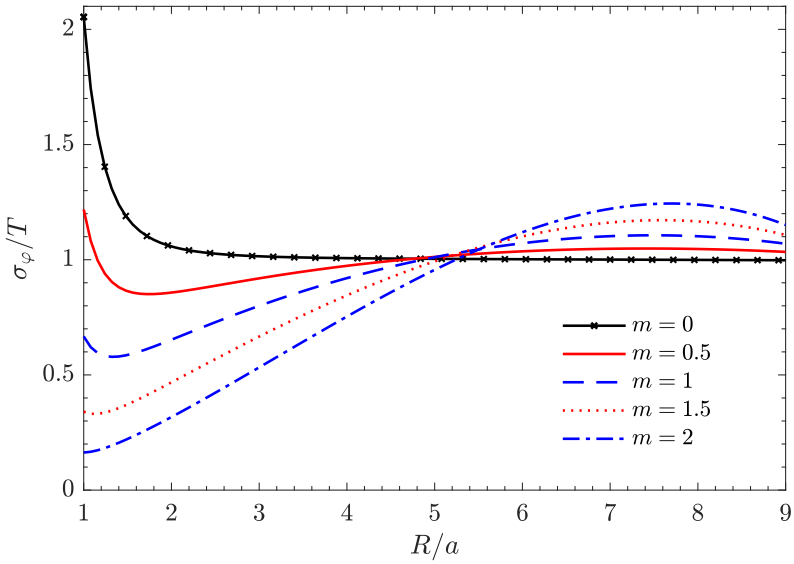

Figure 4. Variation of dimensionless longitudinal stress with radial distance for five grading indices ($b/a = 9$, $\varphi = \pi/2$).

an ideal grading index, the longitudinal stresses at the inner surface and near the outer boundary of the graded sphere become equal to each other, indicating the best longitudinal stress state along the sphere thickness. A simple numerical search reveals that the optimal grading index is $m_{\text{opt}} = 1.28$, at which the highest reduction rate (47.9%) in the maximum longitudinal stress has been achieved. In view of Figure 3, the longitudinal stress for $m_{\text{opt}} = 1.28$ should still have a nonuniform distribution. With the power-law gradation of shear modulus, it is thus impossible to achieve a completely uniformly distributed longitudinal stress. As the grading index becomes higher than the optimal value, the SCF increases again. The effects of the inhomogeneous shear modulus have therefore been weakened to a certain extent.

To investigate the influence of the radii ratio between the outer and the inner surface of the graded thick-walled sphere, we further reexamined the longitudinal stress distribution for the case of $b/a = 9$ (Figure 4). Although the overall distribution patterns are similar to those for the case of $b/a = 3$, the effects of the radii ratio is very clear. For example, when $m = 1$, the maximum longitudinal stress takes at the inner surface of the thick-walled sphere for the radii ratio $b/a = 3$. However, when $b/a = 9$, the maximum stress concentration has shifted to near the outer boundary of the sphere ($R/a = 7.48$). The reduction rate becomes 46.1%, which is higher than the one corresponding to $b/a = 3$. Consequently, for the same grading index, a larger radii ratio tends to drive the high stress zone from the inner boundary toward to the outer surface of the thick-walled sphere and results in a better SCF reduction rate. To validate this hypothesis, we further calculated the maximum longitudinal stress for a few different radii ratios.

Figure 5 shows the variation of the SCF as a function of the radii ratio within the interval $3 \le b/a \le 18$. For all five grading indices, the SCF monotonically decreases as the radii ratio of the graded sphere enlarges. For the homogeneous thick-walled sphere, the maximum longitudinal stress always occurs at its inner boundary for any radii ratio. With increased radii ratio, the SCF rapidly converges to a constant

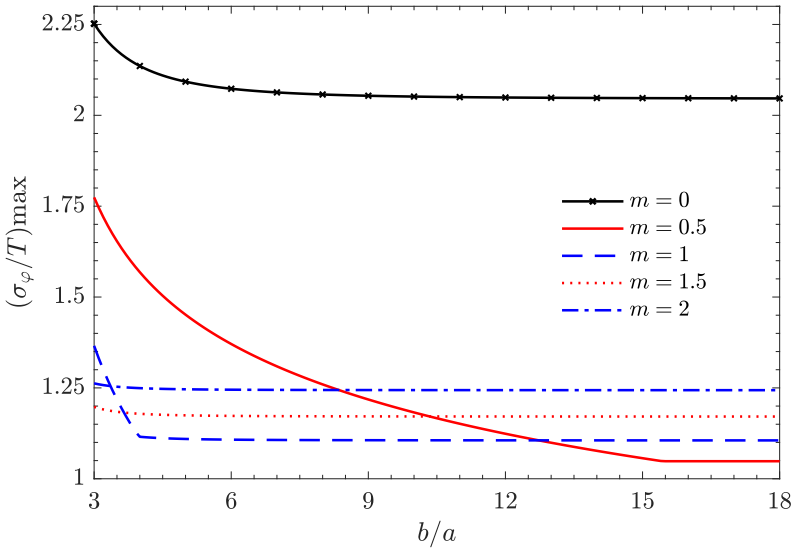

Figure 5. Variation of the maximum longitudinal stress found in the graded sphere as a function of the radii ratio b/a for five grading indices ($\varphi = \pi/2$).

(2.045) that corresponds to the SCF of an infinite hollow sphere ($\nu = 0.3$). As the shear modulus of the thick-walled sphere becomes nonuniform, the maximum longitudinal stress does not necessarily occur at its inner boundary. For the grading index $m = 0.5$ and 1, a corner in the SCF curve can clearly be found at $b/a = 15.5$ and 4.0, respectively. This behavior indicates the fact that the location of the maximum longitudinal stress has shifted from the inner boundary to near the outer surface of the graded sphere. As the grading index further increases to $m = 1.5$, the maximum longitudinal stress appears near the outer surface of the thick-walled sphere for all studied radii ratios $3 \le b/a \le 18$. As a result, the SCF curve for the grading index $m = 1.5$ becomes again very smooth. With increased radii ratio, the SCF rapidly converges to a constant. The corner no longer exists. For the largest considered grading index ($m = 2$), the SCF becomes nearly a constant and thus independent of the radii ratio.

For completeness, we also examined the distribution of the latitudinal stress in the graded thick-walled sphere. Figure 6 shows the variation of dimensionless latitudinal stress along its inner surface for the same five grading indices that have been previously considered. No severe stress concentrations were found, because the direction of the latitudinal stress is always normal to the applied uniaxial tension. Independent of the grading index, the maximum magnitude of the latitudinal stress always occurs on two poles of the inner boundary. It is clear that the maximum latitudinal stress at the inner surface continues to decrease as the grading index increases.

In analogy to Figure 3, Figure 7 shows the distribution of the latitudinal stress along the radial direction. As before, both the analytical and the FE solutions were presented. The disagreement between FE and analytical solutions also increases with the grading index. However, in contrast to the case of longitudinal stress (Figure 3), much better agreements can be found. It is noted that, for all five grading indices, the latitudinal stress climbs monotonically from the inner boundary toward to the outer surface of the thick-walled sphere. The impact of the grading index is very clear. At the inner boundary of the thick-walled

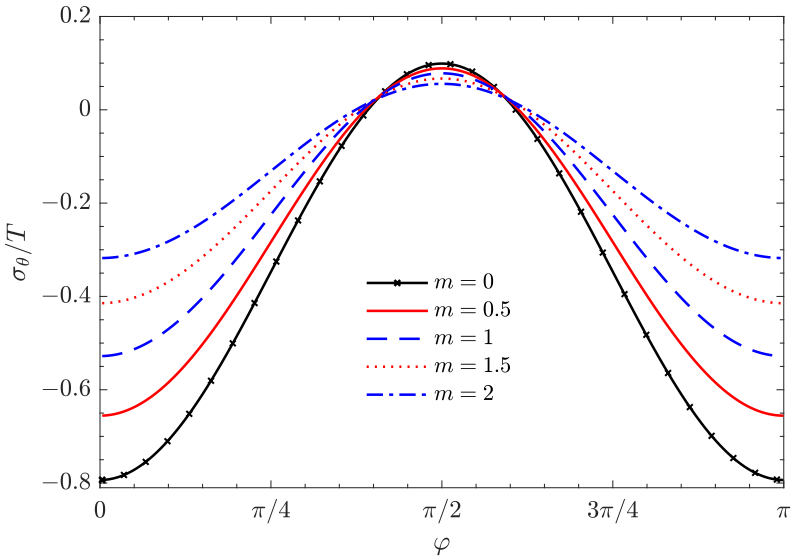

Figure 6. Variation of dimensionless latitudinal stress along the inner surface of the graded thick-walled sphere for five grading indices ($b/a = 3$, $R = a$).

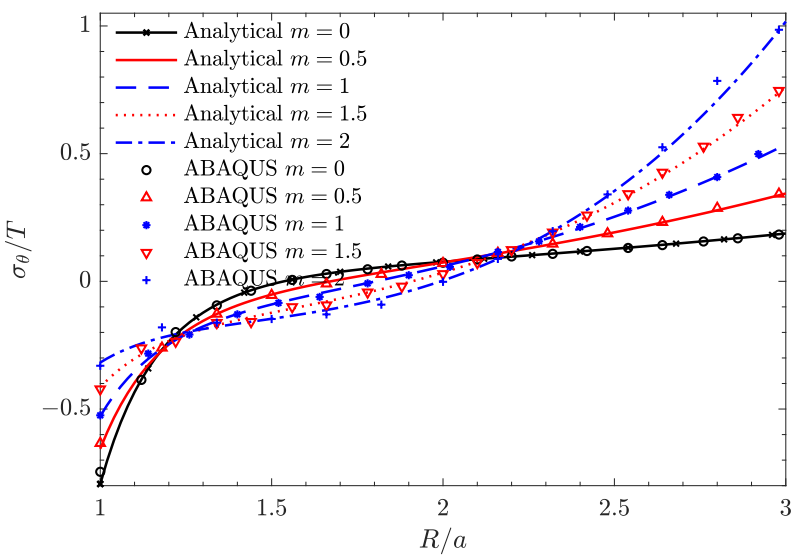

Figure 7. Variation of dimensionless latitudinal stress with radial distance for five grading indices ($b/a = 3$, $\varphi = 0$ or π).

sphere, the latitudinal stress decreases with increased grading index. At the outer surface, the opposite is true. As a balance, the intermediate grading index $m = 1$ seems to be the best choice of the five if the latitudinal stress is of the primary concern. For this particular case, $\sigma_\theta/T = -0.528$ and 0.535, respectively, at the inner and the outer surface of the thick-walled sphere.

m	0	0.25	0.5	0.75	1	1.25	1.5	1.75	2	$m_{\text{opt}} = 0.99$
$\lvert\sigma_\theta\rvert/T$	0.793	0.723	0.656	0.590	0.535	0.644	0.761	0.885	1.017	0.531
Reduction rate	0	8.9%	17.3%	25.6%	32.5%	18.8%	4.0%	−11.6%	−28.2%	33.0%

Table 2. The maximum SCF in latitudinal stress occurring at either boundary of a graded thick-walled sphere under the application of a uniaxial outer tension ($b/a = 3$, $\varphi = 0, \pi$).

Table 2 tabulates the maximum values of the latitudinal stress (in magnitude) in the graded thick-walled sphere for a few representative grading indices. For small grading indices ($m < 0.99$), the magnitude of the latitudinal stress at the inner surface is larger than that at the outer boundary. However, for $m = 0.99$, $|\sigma_\theta|/T$ at the outer boundary becomes equal to the one at the inner surface. Consistent with previous discussions, such a grading index can be defined as its optimal value (m_{opt}). For this case, the highest reduction rate (33.0%) in the maximum latitudinal stress is achieved. With the further increase of the grading index, the latitudinal stress at the outer boundary remains positive and continues to climb. As a result, the reduction rate of $|\sigma_\theta|/T$ starts to decrease. The effects of the inhomogeneous shear modulus on the reduction of latitudinal stress become nearly negligible when the grading index increases to $m = 1.5$. For $m = 2$, the latitudinal stress at the outer boundary of the sphere becomes even far larger than the classical SCF in the latitudinal stress.

Figure 8 shows the variation of the radial stress component along the symmetry axis of the mechanical model for five grading indices. In view of the uniaxial outer tension applied on the thick-walled sphere, it is along this direction ($\varphi = 0, \pi$) that the radial stress takes its maximum value. Both analytical and FE solutions are presented for all five grading indices. As can be observed from the figure, reasonable agreements between the two independent solutions are obtained for the radial stress component. This is

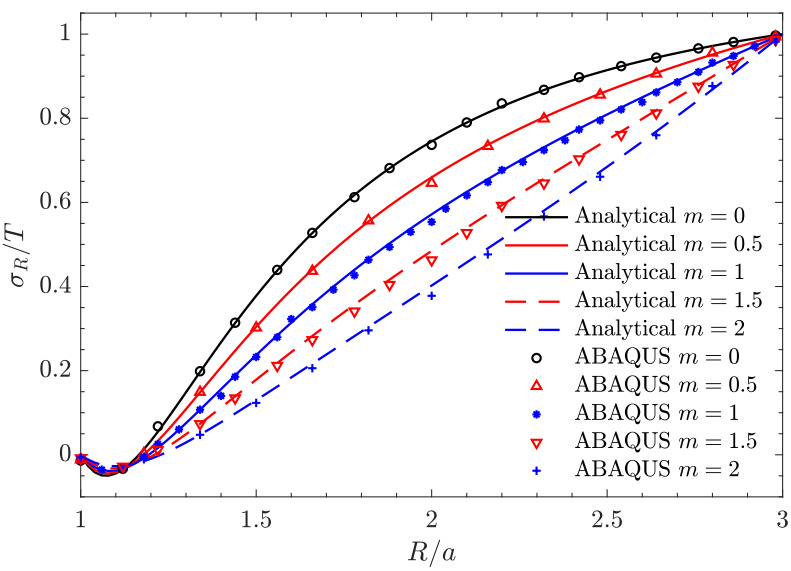

Figure 8. Variation of dimensionless radial stress with radial distance for five grading indices ($b/a = 3$, $\varphi = 0$ or π).

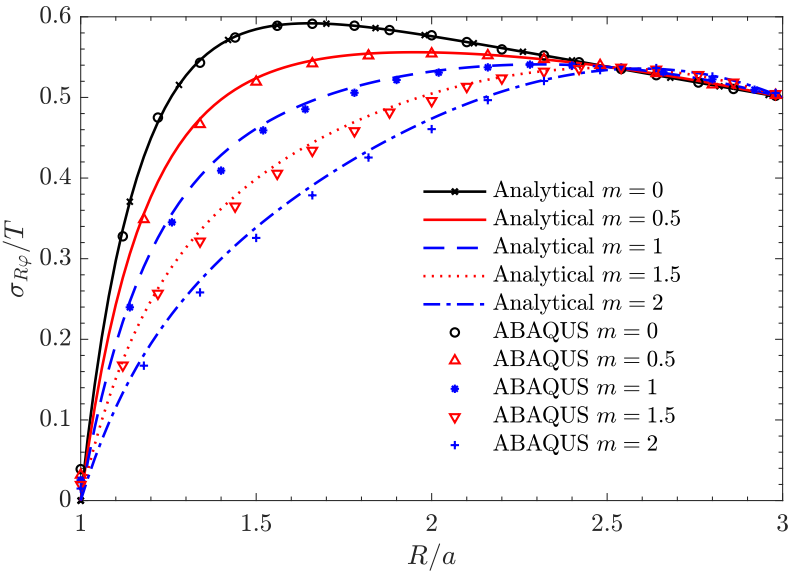

Figure 9. Variation of dimensionless shear stress with radial distance for five grading indices. ($b/a = 3, \varphi = 3\pi/4$)

true even for the largest grading index ($m = 2$), in contrast to the case of longitudinal stress. Limited by the boundary conditions $(3)_1$ and $(2)_1$, the dimensionless radial stress σ_R/T is exactly 0 and 1 at the inner and outer surfaces of the thick-walled sphere. Within the studied range of the grading index $0 \le m \le 2$, no stress concentrations in the radial stress were found. Nonetheless, the introduction of an inhomogeneous shear modulus is able to affect the distribution pattern of the radial stress. With increased grading index, the radial stress between the two boundaries of the thick-walled sphere becomes closer to a linear function of the radial coordinate.

Finally, in Figure 9, we present the variation of the shear stress component along the particular direction $\varphi = 3\pi/4$ for the same five grading indices. It is along this direction that the shear stress takes its maximum positive value. At the inner and the outer surfaces of the thick-walled sphere, the dimensionless shear stress $\sigma_{R\varphi}/T$ is exactly 0 and 0.5, respectively, as given by the boundary conditions $(3)_2$ and $(2)_2$. Similar to the case of radial stress, increasing the grading index helps to straighten the shear stress variation through the thickness dimension of the hollow sphere. As a result, the overall shear stress level becomes lower and lower than its classical counterpart. As before, although the disagreement between FE and analytical shear stresses also increases with the grading index, the discrepancy is acceptable and much less than that of the longitudinal stress.

4. Concluding remarks

In this paper, we successfully developed an analytical solution to a graded thick-walled sphere subjected to a uniaxial outer tension. While the Poisson's ratio of the sphere was fixed as a constant, its shear modulus was allowed to vary as a power-law function of the radial coordinate. The analytical solution was derived through directly tackling the equilibrium equations of displacements of the graded

thick-walled sphere. Informed by the distribution pattern of the applied uniaxial outer tension, function forms of both the radial and the longitudinal displacements were proposed in terms of three unknown functions of the radial coordinate. In this way, the two equations of equilibrium were recast into three differential equations of the Euler type involving the three fundamental unknown functions. The system of second-order differential equations were further reduced into six first-order ones by taking both the three fundamental unknown functions and their derivatives as new unknown variables. The new system is then converted into a first-order differential matrix equation and analytically solved by the joint use of the first-order differential equation theory and the eigenvalue theory. In order to validate the correctness of the derived analytical solution, finite element solution of the graded thick-walled sphere was also calculated and a reasonable agreement between the two independent methods were identified for both the stress distributions and stress concentration factors. On the basis of extensive parametric studies, a few observations and conclusions can be drawn as follows:

- In order to drive the high stress zone conventionally taking place near the inner boundary of a homogeneous thick-walled sphere, the modulus of elasticity of thick-walled spheres should be designed as an increasing function of the radial coordinate.
- In analogy to the case of a homogeneous thick-walled sphere, the longitudinal stress component remains to be the primary concern in the graded ones. No significant stress concentrations were found in latitudinal, radial and shear stresses.
- With increased shear modulus gradation, the high stress zone tends to shift from the inner surface toward to the outer boundary of thick-walled spheres. In contrast to homogeneous thick-walled spheres, for graded ones, two local stress maxima exist. As they become equal, an optimal grading index in the power-lower function of shear modulus can be defined.
- For a given grading index in the power-lower function of shear modulus, the stress concentration factor monotonically decays with increased radii ratio between the outer and the inner surface of the graded sphere and gradually converges to the factor of an infinite hollow sphere. This global maximum stress may occur either at the inner boundary or near the outer surface of the graded sphere, depending on both the radii ratio and the grading index. With increased grading index, a smaller radii ratio is required in order to shift the most sever stress concentration from the inner surface toward to the outer boundary vicinity.

Acknowledgements

This work was supported by the National Natural Science Foundation of China [grant numbers 11872149 and 11472079] and the Fundamental Research Funds for the Central Universities.

References

[Atashipour et al. 2014] S. A. Atashipour, R. Sburlati, and S. R. Atashipour, "Elastic analysis of thick-walled pressurized spherical vessels coated with functionally graded materials", *Meccanica* (*Milano*) **49**:12 (2014), 2965–2978.

[Barati and Jabbari 2015] A. R. Barati and M. Jabbari, "Two-dimensional piezothermoelastic analysis of a smart FGM hollow sphere", *Acta Mech.* **226**:7 (2015), 2195–2224.

[Barber 1992] J. R. Barber, *Elasticity*, Solid Mech. Appl. **12**, Kluwer, Dordrecht, Germany, 1992.

[Bayat and EkhteraeiToussi 2015] Y. Bayat and H. EkhteraeiToussi, "General thermo-elastic solution of radially heterogeneous, spherically isotropic rotating sphere", *J. Mech. Sci. Technol.* **29** (2015), 2427–2438.

[Birman and Byrd 2007] V. Birman and L. W. Byrd, "Modeling and analysis of functionally graded materials and structures", *Appl. Mech. Rev.* (*ASME*) **60**:5 (2007), 195–216.

[Dryden and Batra 2013] J. Dryden and R. C. Batra, "Optimum Young's modulus of a homogeneous cylinder energetically equivalent to a functionally graded cylinder", *J. Elasticity* **110**:1 (2013), 95–110.

[Evci and Gülgeç 2018] C. Evci and M. Gülgeç, "Functionally graded hollow cylinder under pressure and thermal loading: effect of material parameters on stress and temperature distributions", *Int. J. Eng. Sci.* **123** (2018), 92–108.

[Fukui and Yamanaka 1992] Y. Fukui and N. Yamanaka, "Elastic analysis for thick-walled tubes of functionally graded material subjected to internal pressure", *JSME Int. J. Solid Mech. Strength Mater.* **35**:4 (1992), 379–385.

[Ghannad 2013] M. Ghannad, "Elastic analysis of pressurized thick cylindrical shells with variable thickness made of functionally graded materials", *Compos. B Eng.* **45**:1 (2013), 388–396.

[Ghannad and Nejad 2012] M. Ghannad and M. Z. Nejad, "Complete closed-form solution for pressurized heterogeneous thick spherical shells", *Mechanika* **18**:5 (2012), 508–516.

[Ghayesh and Farajpour 2019] M. H. Ghayesh and A. Farajpour, "A review on the mechanics of functionally graded nanoscale and microscale structures", *Int. J. Eng. Sci.* **137** (2019), 8–36.

[Jabbari et al. 2013] M. Jabbari, S. Karampour, and M. R. Eslami, "Steady state thermal and mechanical stresses of a poro-piezo-FGM hollow sphere", *Meccanica* (*Milano*) **48**:3 (2013), 699–719.

[Jabbari et al. 2017] M. Jabbari, S. M. Mousavi, and M. A. Kiani, "Functionally graded hollow sphere with piezoelectric internal and external layers under asymmetric transient thermomechanical loads", *J. Press. Vessel Technol.* (*ASME*) **139**:5 (2017), art. id. 051207.

[Jin and Batra 1996] Z.-H. Jin and R. Batra, "Some basic fracture mechanics concepts in functionally graded materials", *J. Mech. Phys. Solids* **44**:8 (1996), 1221–1235.

[Kubair 2013] D. V. Kubair, "Stress concentration factors and stress-gradients due to circular holes in radially functionally graded panels subjected to anti-plane shear loading", *Acta Mech.* **224**:11 (2013), 2845–2862.

[Kubair and Bhanu-Chandar 2008] D. V. Kubair and B. Bhanu-Chandar, "Stress concentration factor due to a circular hole in functionally graded panels under uniaxial tension", *Int. J. Mech. Sci.* **50**:4 (2008), 732–742.

[Le 2017] K. C. Le, "An asymptotically exact theory of functionally graded piezoelectric shells", *Int. J. Eng. Sci.* **112** (2017), 42–62.

[Li et al. 2018] X. Li, Y. Hua, C. Zheng, and C. Mi, "Tuning stress concentrations through embedded functionally graded shells", *J. Mech. Mater. Struct.* **13**:3 (2018), 311–335.

[Liu et al. 2018] Z. Liu, J. Yan, and C. Mi, "On the receding contact between a two-layer inhomogeneous laminate and a half-plane", *Struct. Eng. Mech.* **66**:3 (2018), 329–341.

[Mohammadi et al. 2011] M. Mohammadi, J. R. Dryden, and L. Jiang, "Stress concentration around a hole in a radially inhomogeneous plate", *Int. J. Solids Struct.* **48**:3-4 (2011), 483–491.

[Nejad et al. 2016] M. Z. Nejad, M. Abedi, M. H. Lotfian, and M. Ghannad, "Exact and numerical elastic analysis for the FGM thick-walled cylindrical pressure vessels with exponentially-varying properties", *Arch. Metall. Mater.* **61**:3 (2016), 1649–1654.

[Nie and Batra 2010] G. J. Nie and R. C. Batra, "Exact solutions and material tailoring for functionally graded hollow circular cylinders", *J. Elasticity* **99**:2 (2010), 179–201.

[Poultangari et al. 2008] R. Poultangari, M. Jabbari, and M. R. Eslami, "Functionally graded hollow spheres under non-axisymmetric thermo-mechanical loads", *Int. J. Press. Vessels Pip.* **85**:5 (2008), 295–305.

[Sburlati 2013] R. Sburlati, "Stress concentration factor due to a functionally graded ring around a hole in an isotropic plate", *Int. J. Solids Struct.* **50**:22-23 (2013), 3649–3658.

[Sburlati and Cianci 2015] R. Sburlati and R. Cianci, "Interphase zone effect on the spherically symmetric elastic response of a composite material reinforced by spherical inclusions", *Int. J. Solids Struct.* **71** (2015), 91–98.

[Sburlati et al. 2014] R. Sburlati, S. R. Atashipour, and S. A. Atashipour, "Reduction of the stress concentration factor in a homogeneous panel with hole by using a functionally graded layer", *Compos. B Eng.* **61** (2014), 99–109.

[Sburlati et al. 2017] R. Sburlati, M. Kashtalyan, and R. Cianci, "Effect of graded interphase on the coefficient of thermal expansion for composites with spherical inclusions", *Int. J. Solids Struct.* **110-111** (2017), 80–88.

[Sburlati et al. 2018] R. Sburlati, R. Cianci, and M. Kashtalyan, "Hashin's bounds for elastic properties of particle-reinforced composites with graded interphase", *Int. J. Solids Struct.* **138** (2018), 224–235.

[Suresh et al. 1999] S. Suresh, M. Olsson, A. E. Giannakopoulos, N. P. Padture, and J. Jitcharoen, "Engineering the resistance to sliding-contact damage through controlled gradients in elastic properties at contact surfaces", *Acta Mater.* **47**:14 (1999), 3915–3926.

[Tutuncu 2007] N. Tutuncu, "Stresses in thick-walled FGM cylinders with exponentially-varying properties", *Eng. Struct.* **29**:9 (2007), 2032–2035.

[Tutuncu and Ozturk 2001] N. Tutuncu and M. Ozturk, "Exact solutions for stresses in functionally graded pressure vessels", *Compos. B Eng.* **32**:8 (2001), 683–686.

[Xin et al. 2014] L. Xin, G. Dui, S. Yang, and J. Zhang, "An elasticity solution for functionally graded thick-walled tube subjected to internal pressure", *Int. J. Mech. Sci.* **89** (2014), 344–349.

[Yan and Mi 2019] J. Yan and C. Mi, "A receding contact analysis for an elastic layer reinforced with a functionally graded coating and pressed against a half-plane", *J. Mech. Sci. Technol.* **33**:9 (2019), 4331–4344.

[Yan et al. 2019] J. Yan, C. Mi, and Z. Liu, "A semianalytical and finite-element solution to the unbonded contact between a frictionless layer and an FGM-coated half-plane", *Math. Mech. Solids* **24**:2 (2019), 448–464.

[Yang and Gao 2016] Q. Yang and C.-F. Gao, "Reduction of the stress concentration around an elliptic hole by using a functionally graded layer", *Acta Mech.* **227**:9 (2016), 2427–2437.

[Yang et al. 2009] Q. Yang, C.-F. Gao, and W. Chen, "Stress analysis of a functional graded material plate with a circular hole", *Arch. Appl. Mech.* **80**:8 (2009), 895–907.

[Yang et al. 2015] B. Yang, W. Q. Chen, and H. J. Ding, "3D elasticity solutions for equilibrium problems of transversely isotropic FGM plates with holes", *Acta Mech.* **226**:5 (2015), 1571–1590.

[Zheng et al. 2019] C. Zheng, X. Li, and C. Mi, "Reducing stress concentrations in unidirectionally tensioned thick-walled spheres through embedding a functionally graded reinforcement", *Int. J. Mech. Sci.* **152** (2019), 257–267.

Received 17 Jan 2020. Revised 18 Jul 2020. Accepted 12 Aug 2020.

CHENYI ZHENG: 594040623@qq.com
Jiangsu Key Laboratory of Engineering Mechanics, School of Civil Engineering, Southeast University, 2 Sipailou Street, Nanjing, 210096, China

CHANGWEN MI: mi@seu.edu.cn
Jiangsu Key Laboratory of Engineering Mechanics, School of Civil Engineering, Southeast University, 2 Sipailou Street, Nanjing, 210096, China

JOURNAL OF MECHANICS OF MATERIALS AND STRUCTURES

msp.org/jomms

Founded by Charles R. Steele and Marie-Louise Steele

Cover photo: Wikimedia Commons

See msp.org/jomms for submission guidelines.

JoMMS (ISSN 1559-3959) at Mathematical Sciences Publishers, 798 Evans Hall #6840, c/o University of California, Berkeley, CA 94720-3840, is published in 10 issues a year. The subscription price for 2020 is US $660/year for the electronic version, and $830/year (+$60, if shipping outside the US) for print and electronic. Subscriptions, requests for back issues, and changes of address should be sent to MSP.

JoMMS peer-review and production is managed by EditFLOW® from Mathematical Sciences Publishers.

PUBLISHED BY

mathematical sciences publishers

nonprofit scientific publishing

http://msp.org/

Journal of Mechanics of Materials and Structures

Volume 15, No. 5 December 2020

Approximate conformal mappings and elasticity problems for noncircular tubes
Damir F. Abzalilov, Pyotr N. Ivanshin and Elena A. Shirokova 555

Magnetorheological elastomer isolator in compression mode for IMU vibration isolation
Yang Fufeng and Tao Yu 565

Analytical solutions for displacements and stresses in functionally graded thick-walled spheres subjected to a unidirectional outer tension
Chenyi Zheng and Changwen Mi 585

Field intensity factors of three cracks originating from a circular hole in a thermoelectric material
Qing-Nan Liu and Sheng-Hu Ding 605

Experimental study of deformation processes in large-scale concrete structures under quasistatic loading
Igor Shardakov, Irina Glot, Aleksey Shestakov, Roman Tsvetkov, Valeriy Yepin and Georgiy Gusev 619